Journal of
Ceramic Science
and Technology

*J. Ceram. Sci. Technol.*, **13** [2] 65-82 (2022)
DOI: 10.4416/JCST2021-00015
available online at: http://www.ceramic-science.com


# Plots of Surface Temperature and Mass of a Heated, Large Limestone Sample in Terms of Regression Splines and the Programming Language R

**R. Lech**[1], **S. Sado***[2]

[1]AGH University of Science and Technology in Cracow
[2]Zakłady Magnezytowe "ROPCZYCE" S.A. Research and Development Centre of Ceramics
received August 3, 2021; received in revised form July 27, 2022; accepted August 3, 2022

**Abstract**

**The use of the surface temperature and the mass of a limestone sample or sample conversion degree as variables present in various models of limestone calcination is shown in the paper. The linear model of the thermal dissociation rate of a large limestone sample is derived using the R program and the base of B -splines. The statistical significance of the formulated model is demonstrated. The example of the model recording of the thermal dissociation rate of a large limestone sample as a function of heating conditions, including the sample heating time, is shown. The values of the basis functions contained in the regression matrix have been identified. Moreover, the formulas for non-zero cubic basis functions in the selected span knot of the explanatory variable are derived.**

*Keywords: Limestone, thermal dissociation, thermal analysis, statistical modelling, regression splines*

## I. Introduction

Modelling of the process of limestone thermal decomposition in industrial kilns was initiated by Zawadzki and Bretsznajder [1–5] based on the course of the reaction in single-variable reaction systems:

$$A_{solid} + B_{gas} \leftrightarrows C_{solid} \quad (1)$$

in which, i.a, the equilibrium $CO_2$ pressure of the system:

$$CaCO_3 \leftrightarrows CaO + CO_2 + \Delta H_T^{\circ} \quad (2)$$

was studied as a function of system temperature, and $\Delta H_T^{\circ}$ is the enthalpy of dissociation of calcium carbonate at temperature T.

Hills [6] studied the thermal dissociation mechanism of spheres with diameters of about 1.1 cm and 2.3 cm, made of calcite grains compressed and sintered in a $CO_2$ atmosphere. In his experiments, he measured the temperature at the geometric centre of the thermally dissociated sample and its mass. The sample was dissociated in a stream of air mixture with a known content of carbon dioxide. He generalised the results of his experiments into three models of thermal dissociation of samples, which relate the $CO_2$ pressure at the reaction front to the temperature of the front. They are:

- model of linear dependence of the partial pressure of $CO_2$ at the reaction front on the reaction front temperature, derived with the assumption of a small difference between the temperature of the gaseous mixture surrounding the dissociated sample and the temperature of the dissociation reaction front occurring inside the sample
- model of exponential dependence of the partial pressure of $CO_2$ at the reaction front on the temperature of the front resulting from the van't Hoff isotherm [7],
- the pseudo-steady-state model, which takes into account the heat needed to heat the dissociating sample from the initial temperature to the temperature of the dissociation reaction front.

The above models relate the rate of the reaction front movement to the reaction front temperature and the temperature of the gas mixture surrounding the decomposed sample. In the derivation of the equations of the above models, the equality of the sample surface temperature and the temperature of the gas mixture surrounding the thermally dissociated sample was assumed. The shrinking core model [8] was assumed in the description of the thermal dissociation reaction front of the samples.

Verma [9] used the shrinking core model in both describing the thermal dissociation reaction of a 10-cm-diameter spherical limestone charge and the combustion of a 5-cm-diameter spherical coal grain in a coal-fired shaft kiln for lime production. The temperature of the dissociation front was related to the surface temperature of the dissociated charge in the model equation for the conducted heat flux to the thermally dissociated limestone sphere. This flux is the sum of the heat needed for the thermal dissociation reaction of the limestone and the heat needed to heat the arising calcium oxide layer.

Khinast *et al.* [10] modelled the influence of the partial pressure of $CO_2$ and the size of limestone grains on their

* Corresponding author: sebastian.sado@ropczyce.com.pl

thermal dissociation rate limited by the chemical reaction rate and/or by the diffusion of carbon dioxide in the grain pores. The model of thermal dissociation of limestone grains derived by Khinast *et al.* [10], called the reacting particle model, is the result of thermal dissociation studies of limestone grains containing 96.1 wt% $CaCO_3$, 1.8 wt% $MgCO_3 + H_2O$, 2.1 wt% inert substance. Furthermore, the average grain diameters of the three studied fractions were: 7.5 μm, 56.5 μm and 90 μm. The model differs from the shrinking core model by assuming thermal dissociation of the particles occurring not only on a spherical surface of the reaction front, but also the formation of carbon dioxide in the network of pores present in limestone and evolving during thermal dissociation of the particle. In addition, the model assumes the existence of a boundary layer at the surface of the reacting particle, called a gas film, and the invariability of the grain diameter. The model mass transport equations include the conversion rate taking into account the change in mass of the calcined particle. In turn, the equation of heat transport to the surface of the dissociating particle contains the particle surface temperature. The system of model equations also includes an equation for the rate of reaction containing a parameter $K$ depending on the value of a function of carbon dioxide partial pressure $f(CO_2)$ and calculated from the formula:

$$K = k \times f(CO_2) \tag{3}$$

where: $k$ is the rate constant for the reaction.

The course of thermal dissociation process of limestone particles is important for the quality of produced lime. Lime is a basic chemical product with many applications. Hence, the interest of technologists and designers in the lime industry in the organisation of lime firing. Boynton [11] lists ten critical variables affecting lime quality and productivity. Among these variables, he considers the calcination rate and the temperature and duration of calcination to be the variables of the highest importance, which is consistent with the conclusions drawn from the models discussed above, which focused on the movement of the reaction front in the particle.

He emphasises that each limestone is characterised by its own properties, which means that the process parameter values for a particular limestone and kiln are generally selected based on the trial and error method. Otherwise, the results of thermal dissociation of the limestone, including product quality, are unpredictable.

A similar point of view is held by Oates [12] considering the transport of heat to the reaction front and the transport of released carbon dioxide to the outside of the calcined particle. He states that the most important variables on which the output and quality of the produced lime depend are the temperature distribution in the calcination zone and the rate of heat transfer between the calcined particle and its surroundings.

Mathematical modelling of the thermal dissociation of limestone raw meal occurring in a rotary kiln for the production of cement clinker is a very difficult issue due to the complexity of heat transfer processes, mass transport, chemical thermodynamics, and mineralogical reactions.

Locher [13, 14] built a mathematical model of cement clinker production using heat and mass balance. He formed the model primarily due to the significance of the influence of respective variables on the calculated steady-state parameters of all processes and unit operations involved in cement clinker production. He distinguished the temperature of grains of calcined raw meal assuming the equality of this temperature with the temperature of gases surrounding the particles during calcination. Particles of calcined raw meal are very finely ground, e.g. in a stream of these particles, the residue on a sieve with 4 900 mesh/cm$^2$ is less than 10 %. Another important parameter of the model is the degree of thermal dissociation of $CaCO_3$, which results in the formation of CaO depending on the temperature of the charge flux.

Martins *et al.* [15, 16] developed a one-dimensional steady-state model of the calcination of a limestone charge in a rotary kiln. He included differential equations for mass and heat balance in the model and used the Hills model [6] to calculate the thermal dissociation rate of charge particles with diameters up to about 23 mm. In the equations of heat exchange occurring in the rotary kiln volume between the gas filling it, the charge particles, and the inner wall of the kiln, one of the variables is the particle surface temperature. The model allows the evaluation of the impact of changes in the furnace operating parameters on its efficiency and product quality.

Modelling of the thermal dissociation of the charge in a shaft kiln for lime production and optimising the kiln design together with optimising the process parameters is the subject of work by Gordon *et al.* [17, 18]. The system of model equations includes the mass exchange equation, in which the rate of thermal dissociation of the charge depends, among other things, on the surface temperature of dissociated lumps (particles) of charge. In turn, the assumption of a vortexless flow of gases in the furnace shaft and the introduction of the stream function $\psi$ into the model enable the optimisation of its design and operation.

In their analysis of calcination models of fine limestone particles, Stanmore *et al.* [19] consider the influence of limestone properties on the calcination process and the properties of the product, the kinetics of the process, the effect of carbon dioxide, water vapour and particle size on the calcination rate. The shape of the reaction front assumed in the model affects the dependence of the dissociation rate on the local concentration of carbon dioxide, which is directly unmeasurable. Therefore, depending on the kind of calcined limestone, different reaction front models are used, including a grain model with changing size [20].

In the analysis of calcination of limestone in the calcination zone of a shaft furnace, Bes [21] adopted the shrinking core model to describe the shape of the dissociation reaction front. The system of model equations included the heat balance for the gas and charge fluxes flowing in the furnace shaft and the limestone dissociation rate equation. The temperature distributions of: the surface of the calcined charge lumps, the gas mixture, and the core of the calcined charge lumps were the result of solving of the system. Calculation of the above temperature distributions requires a number of iterations to achieve convergence

of the assumed and calculated charge conversion rates in the calcination zone. The need for the iterative calculation method resulted from the assumption of the amount of heat consumption in each shaft zone.

Thermal dissociation of calcium carbonate [2] is a reversible topochemical reaction [22] in which in the parent calcium carbonate crystal structure $CaCO_3$ the ions $CO_3^{2-}$ are changed to $O^{2-}$ ions with the liberation of gaseous $CO_2$ which causes heterophase fluctuations [1–5]. The formation of such fluctuations is mainly possible in areas of disorder on the surface of the dissociated crystal or in the near-surface layer. The liberated $CO_2$ molecules can come not only from the surface of the crystal but also from deeper places. In general, thermal dissociation starts at the surface of the crystal and moves to its centre.

The liberated $CO_2$ on the thermal dissociation front of limestone, e.g. in a shaft furnace, is removed from the surface of a calcined lump by the gas mixture stream flowing in the furnace shaft. The transport of $CO_2$ from the surface of the calcined lump by the gas stream flowing around the lumps is called Stefan flow [23]. Diffusion of $CO_2$ from the surface of the calcined lump to the flowing gas mixture also occurs due to the concentration difference of $CO_2$ on the surface of calcined limestone lump and in the stream of the gas mixture flowing around the lump. Therefore, the total removal flux of $CO_2$ contains two components resulting from: the Stefan flow and the diffusive flow described by Fick's law.

Specht's work [23] includes a mathematical model of the thermal dissociation of a limestone charge in a shaft furnace. In this model, a shrinking core model is used to describe the reaction surface, which takes into account the thermal dissociation reaction properties of the calcium carbonate crystal discussed above. The removal of $CO_2$ from the calcined grain surface by Stefan flow and diffusive flow was also assumed. The set of eight equations included in the model is used to determine the parameters sought, including the surface temperature of calcined grain and radius of the unreacted core, which is the measure of the dissociation ratio. The study of the temperature front of the thermal dissociation reaction of large grains with a diameter of 25 mm originated from different limestones and carried out at 1 050 °C in air shows that the rate of the process is limited by heat transport and reaction kinetics. On the other hand, in the case of calcination of fine grains with a size measured in μm, the thermal dissociation process is limited by the chemical reaction rate. The same happens in the low temperature range of thermal dissociation.

In the work by Hallak *et al.* [24, 25, 26], a system of equations of a one-dimensional mathematical model of heating a spherical charge in a shaft furnace is written. The model consists of ordinary differential equations derived from mass and heat balances prepared for a charge layer of thickness *dz* and a stationary state. The *z* coordinate is calculated on the charge thickness. A shrinking core model was adopted to describe the thermal dissociation of the charge grains. It was assumed that fuel and secondary air are introduced at the same level uniformly across the cross-section of the charge. The uniformity of the temperature distribution of the gas mixture and the charge temperature, as well as the degree of charge conversion in the cross-section of the shaft, was assumed. As a result of the calculations, according to the model, axial temperature distributions of the gas mixture, the surface of the calcined charge, the core of the grains, the average temperature of the grains and the degree of conversion of the charge are obtained. The model is used to optimise the calcination of charge from the point of view of heat consumption and the quality of product. It is also used to train kiln operators. It can be used to analyse the influence of parameters such as grain size distribution of the charge, heat input to the furnace shaft, furnace output, type of fuel used, properties of the limestone to be calcined, etc. on the calcination process and lime quality. Lime firing is a highly energy-intensive thermal process in any lime production method. Therefore, optimization of lime firing is essential as, according to Piringer [27], the firing costs make up 20 – 50 % of the production costs, and in order to protect the environment.

Optimising the thermal efficiency of the process is currently achieved mainly based on mathematical modelling of:

- the firing process taking into account the modelling of thermal dissociation of limestone occurring inside the calcined grain,
- flow of gas and charge fluxes in furnace shaft,
- shape of the furnace shaft.

The above-cited models of thermal dissociation of calcite or limestone grains always include two variables in their system of equations: the surface temperature of the thermally dissociated grain and its actual mass or degree of conversion. The surface temperature of the calcined charge grain can be a given variable or a variable known from measurements in design and optimisation calculations. It can also be a variable calculated on the basis of a system of furnace model equations with assumptions concerning, e.g. the distribution of heat flux entering the charge.

Changes in the properties of a substance caused by transferred heat are studied with thermal analysis methods discussed e.g. by Brown [28]. In these methods, the change in a tested substance property is recorded as a function of the temperature of the substance and the conditions under which the substance is heated or cooled.

Hence, the aim of this paper is to apply the one-dimensional method of splines, which is part of the nonparametric regression included in the works by e.g. Hastie *et al.* [29], Trzęsiok *et al.* [30], for a description of surface temperature or mass variation of a calcined limestone large sample as a function of thermal dissociation time. Statistical modelling of the distributions of these variables over time was carried out using the R language and computing environment [31] for statistical calculations and drawing up plots to facilitate their interpretation.

As already mentioned, this approach can also be used for analytical description of the results obtained with different thermal analysis methods.

**Table 1:** Chemical composition of the marble.

| Loss on ignition (1 000 °C/1h)* [%] | Moisture content (105 °C) [%] | $SiO_2$ [%] | Content of insoluble residue [%] | $Fe_2O_3$ [%] | $Al_2O_3$ [%] | CaO [%] | MgO [%] | $SO_3$ [%] | Sum [%] |
|---|---|---|---|---|---|---|---|---|---|
| 43.70 | 0.03 | 0.12 | 0.00 | 0.0 | 0.09 | 55.30 | 0.64 | <0.02 | 99.85 |

*Moisture content is included in the loss on ignition.

**Table 2**: Density, apparent density, volume of macro- and micropores, total porosity of the marble.

| Density | | Apparent density | | Volume of macro and micropores | Total porosity |
|---|---|---|---|---|---|
| Mean value $\overline{\rho}$ $g/cm^3$ | Standard Deviation $S_\rho$ $g/cm^3$ | Mean value $\overline{\rho}_\alpha$ $g/cm^3$ | Standard Deviation $S_{\rho_\alpha}$ $g/cm^3$ | $V_{por.}$ $cm^3/g$ | ω % |
| 2.74 | 0.002 | 2.74 | 0.004 | 0.00 | 0.00 |

## II. Experimental

### *(1) Materials*

The samples were made of the Precambrian calcite marble "White Marianna", which is a crystalline, coarse-grained precious marble. It is white with shades of grey and brown [32]. The chemical composition of the marble was determined according to the standard "Limestone and unslaked and hydrated lime -chemical analysis" PN -76/B -04350. The results of the analysis are summarised in Table 1 [33].

The density of the marble was determined with the helium method using a Micromeritics AccuPyc 1330 helium pycnometer. The volume of the samples was determined using pure helium. Before measurement, the samples were pre-desorbed by rinsing ten times with pure helium. Five measurements were taken for each sample. The apparent density was determined with the powder method using a GeoPyc 1360 density analyser from Micromeritics. DryFlo powder was used to determine the apparent density. The instrument was calibrated using model shapes. The measurement series consisted of ten measurements. The analysis of the total volume of macro- and mesopores was also performed and the total porosity of the marble was determined. The results of the measurements are summarised in Table 2 [34]. These are within the value ranges of rock physical properties reported in the literature [32].

### *(2) Method of thermal decomposition of the sample*

A marble sample with a diameter d ≅ 49.2 mm shown in Fig. 1. was used in the experiment. The sample is cylindrical in shape with a diameter-to-height ratio of approximately 0.97. A shallow hole is drilled in the specimen sidewall for fastening of the S-type thermocouple junction (PtRh10%-Pt, PN-EN 60584 – 1:2014 – 04) for measuring the surface temperature of the sample. The sample is placed in a vertical cylindrical heating chamber of an electric furnace. A heated mixture of air and carbon dioxide with $c_{CO_2}$ = 45.16 % flows into the chamber. The furnace is equipped with a digital indicating controller FCD -100 from Shinko with a sensor type S and fuzzy self-tuning PID. The controller is used to modify the temperature of the heating chamber based on input of the values for the heating time and the heating chamber temperature are shown in Fig. 2. During calcination of the sample, the temperature at the side of the sample and the current weight of the sample i.a. are recorded. The temperature and mass readings of the calcined sample were taken at equal approximately 90-second intervals. A detailed description of the experiment is included in Lech [33, 34].

## III. Results

### *(1) Sample surface temperature variability during thermal dissociation*

Fig. 3. shows a scatterplot of the temperature measurement results at a selected point on the surface of the heated sample. The plot was made using plot(x, y, …), points(x,y, …) and the par() and legend() functions of the R program:

```
> par(mar=c(5.1,4.1,4.1,2.1)+0.1)
> legend(11500,600,legend=c("measurement point"),pch=1,cex=1.4,col="black",bty="n")
```

The scatterplot of the measured points of the heated sample surface temperature is similar to the plot of the furnace heating curve shown in Fig. 2. During the thermal dissociation period of the sample, the heat consumption by the energy-consuming thermal dissociation reaction of calcium carbonate is so large that the arrangement of measuring points during part of the thermal dissociation period is convex in the direction opposite to the direction of the ordinate axis. This observation will be taken into account during the choice of the degrees of freedom number of the polynomial splines bs() and the natural cubic splines ns() contained in the computational environment R. The wave-shaped arrangement of the sample surface temperature measurement points, visible mainly during the preheating period, is caused by thermal inertia of the furnace heating system and auto-tuning of the temperature controller.

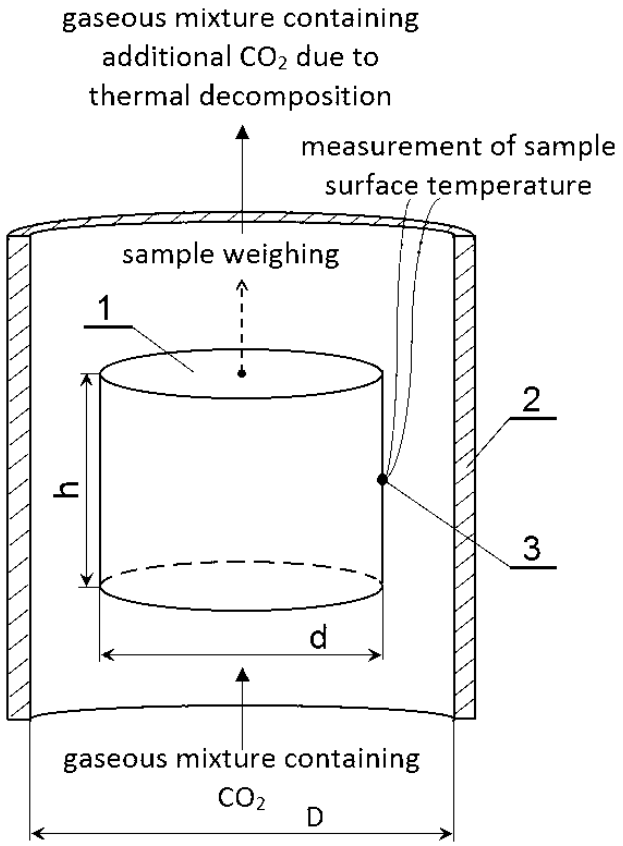


**Fig. 1:** Scheme of heating system for measurement of the mass and surface temperature of a thermally dissociated limestone sample in a heating chamber: 1 – cylindrical sample, 2 - cylindrical wall of the heating chamber, 3 – thermocouple junction.

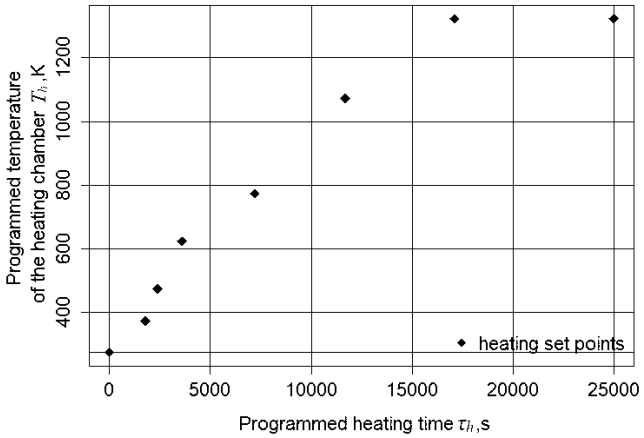


**Fig. 2:** The heating time and heating chamber temperature values programmed in the temperature controller.

### *(2) Sample mass variability during thermal dissociation*

The scatterplot of the measurement points of the heated sample mass is shown in Fig. 4. Thermal dissociation of the sample was performed until the mass of the sample was fixed, as is visible in this plot. In the first part of the thermal dissociation period of the sample, it can be seen that the scatter of the measurement points indicates a convexity of the plot of the relationship under study in the ordinate axis direction. However, the direction of the convexity is changed in the second period of calcination. The above observation will be used in selecting the degrees of freedom number of functions bs() and ns() when plotting the dependence of calcined sample mass vs. calcination time.

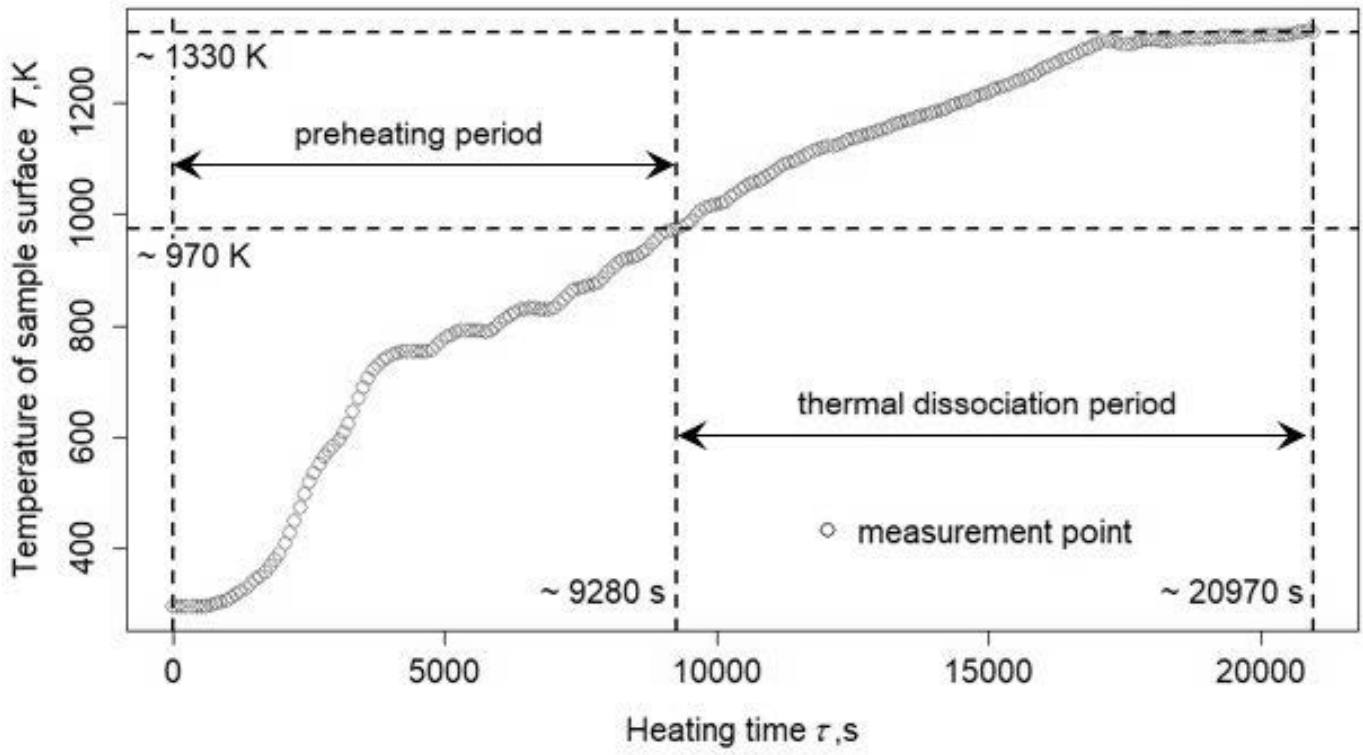


**Fig. 3:** Scatterplot of the surface temperature measurement results of heated sample vs. heating time.

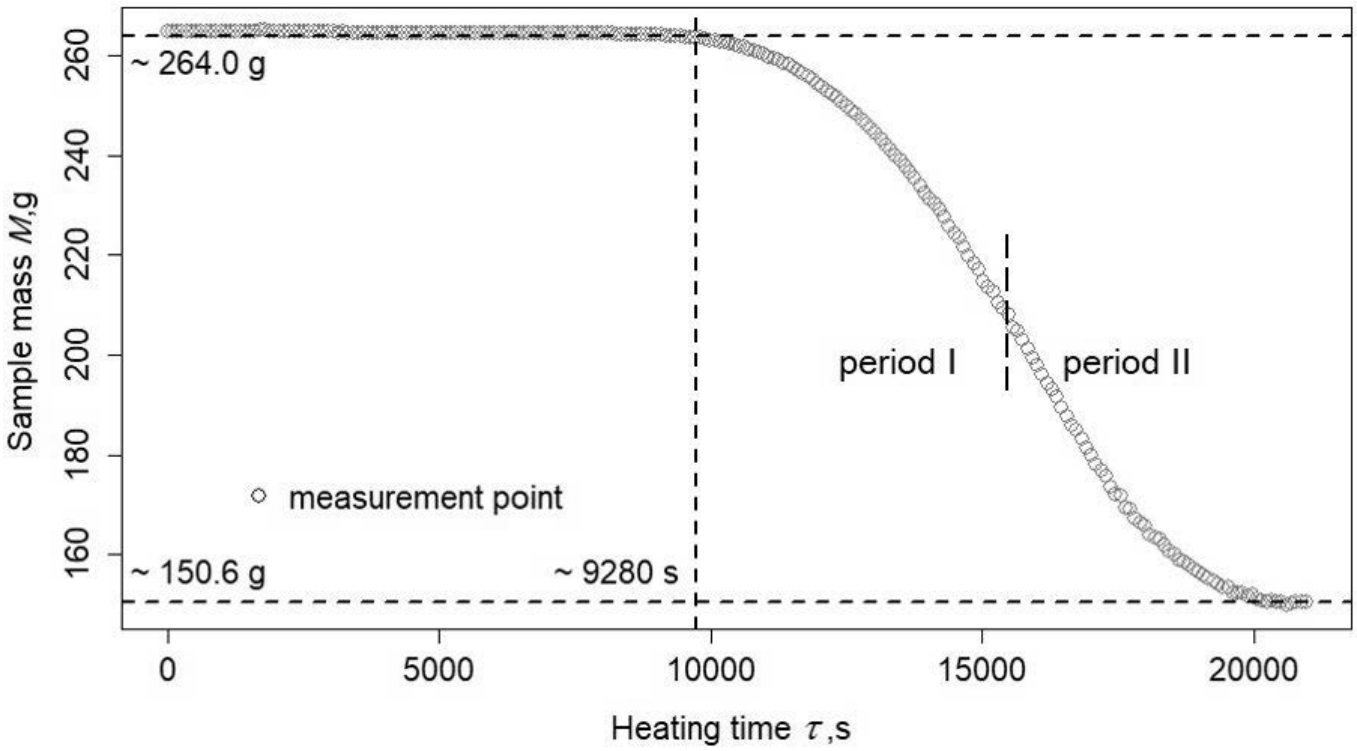


**Fig. 4:** Scatterplot of the mass measurement results of heated sample vs. heating time.

## IV. Discussion

### *(1) Concise about nonparametric regression and splines of degree M and knots $\xi_j$, j = 1,2,..., K, that is, with B-splines as a nonparametric regression method using the programming language R*

The regression analysis, discussed, e.g. by Aczel *et al.* [35], Neter *et al.* [36], of the relationship under study performed using the least squares error method requires that the error components $\varepsilon_i$ in successive observations $x_i$ meet the following assumptions:

- the error components $\varepsilon_i$ are normally distributed,
- the expected value of the error components $\varepsilon_i$ is $E\{\varepsilon_i\} = 0$,
- the variance of the error components $\varepsilon_i$ is constant, i.e., $\sigma^2\{\varepsilon_i\} = \sigma^2$,
- the error components $\varepsilon_i$ of the successive observations $x_i$ are statistically independent.

Non-parametric regression methods, including the regression splines used in this paper to build a regression model of the thermal dissociation rate of a limestone sample vs. a random explanatory variable, i.e. a sample surface temperature, do not require the above-mentioned assumptions relating to the random components of regression model. As Trzęsiok *et al.* [30] point out, when applying these methods, it is not necessary to know the analytical form of the relationship between the response variable and explanatory variable. The nonparametric approach to regression consists in choosing the sought function $f(X_t|\beta_t)$ from the family of smooth functions, where $X_t$ is the explanatory variable and $\beta_t$ is its parameter. Therefore, in this case, the number of possible model fits to the given data set is much larger, as Faraway [37] points out. This is used in the construction of nonlinear models or in cases where there is, e.g., a correlation between explanatory variables. In statistics, splines are used for analytical description of the shape of flexible curves or flexible curved surfaces.

The calculations necessary for the aforementioned application of the method were performed using bs() and ns() functions included in the popular R computing environment, widely used in university teaching of statistics. Following the publication of the paper by Hastie *et al.* [38], advances in computational methods have resulted in the consolidation of spline modelling in statistical regression analysis. In particular, this approach is suitable for statistical modelling of nonlinear dependences of continuous variables using cubic splines.

The purpose of regression splines is to express the response variable Y using a piecewise polynomial spline f(X). The degree of the splines, the number of knots, and their position is determined with this method. In addition, the family of splines is parameterised by taking the number of basis functions or the number of degrees of freedom.

Let X be a vector of length N of an explanatory quantitative variable with non-decreasing real values $X \in \mathbb{R}$ contained in the interval $x_i$ Î [a, b]. The domain of the variable X is divided by a knot sequence $\boldsymbol{\xi} = (\xi_1, \ldots, \xi K)$ such that $\xi_1 \le \xi_2 \le \ldots \le, \xi_K$ into disjoint intervals $[\xi_j, \xi_{j+1})$ with K ≤ N. The points $\xi_j$ are called knots. The smallest and largest values of the domain X are called the boundary knots and are written in terms of $\xi_0$ and $\xi_{K+1}$. In each interval defined by the knots ξj, the piecewise polynomial spline sought is written using different polynomial functions of the form:

$$Y = \alpha_0 + \alpha_1 X + \ldots + \alpha_{d-1} X^{d-1} + \alpha_d X^d \qquad (4)$$

where: $\alpha_d$ is a coefficient, where d = 0,1, … , M-1 is the degree of a partial polynomial in the interval $[\xi_j, \xi_{j+1})$ and M

is the degree of the piecewise polynomial spline generally taking the values 1, 2, 4.

**Definition of spline**

A spline of degree M with knots $\xi_j$, where j = 1,…,K, is a piecewise polynomial function of degree M with continuous derivative up to degree (M -2), with M = 4 for cubic splines as pointed out by e.g. Hastie *et al.* [29], Lis [39], and de Boor [40]. Restricting ourselves to the univariate function, where $X \in \mathbb{R}$ , the spline f(X) is a smooth function of the form of a power series:

$$f(X) = \sum_{m=1}^{M} \beta_m X^{m-1} + \sum_{j=1}^{K} \vartheta_j \left(X - \xi_j\right)_+^{M-1} \tag{5}$$

where: $\beta_m$, $\vartheta_j$ are coefficients, m = 1, …, M, and furthermore:

$$\left(X - \xi_j\right)_+ = \begin{cases} X - \xi_j & if\ X > \xi_j \\ 0 & if\ X \le \xi_j \end{cases} \tag{6}$$

Additional restrictions can be imposed on the above function in the form of linearity of this function beyond the edge nodes. Then for $X < \xi_1$ and $X > \xi_K$, it is assumed that the second derivative in these nodes is zero, i.e. $f''\left(\xi_1^-\right) = 0$ and $f''\left(\xi_K^+\right) = 0$ . The spline obtained under these assumptions is called a natural cubic spline.

A trade-off has to be considered for splines between increasing the number of knots, which may lead to an overfitting of the model to the data and an increase in variance and decreasing the number of knots, which in turn may result in a higher model bias.

**B – spline basis for polynomial splines**

The B - splines set consisting of polynomial splines is called the B – splines base. Let the unknown function f(X) be estimated using a spline with the assumed internal knots vector $\xi$ and degree M = d+1, which can be written with the equation:

$$f(X) = \sum_{j=1}^{K+d+1} \beta_j B_j(X) \tag{7}$$

where: $B_j$ is the set of basis functions and $\beta_j$ are the coefficients associated with these functions.

Thus, Equation [7] is linear due to the coefficients βj, which reduces the estimation of the function f(X) to a linear optimization problem in the transformed variables $B_1(X), B_2(X),\ldots, B_{K+d+1}(X)$. Thus, modelling of the function f(X) using splines reduces to the estimation of a small set of coefficients.

Splines of assumed degree with fixed knots are called regression splines. Fixing the number of knots involves choosing their position. The most commonly used are cubic splines of degree M = 4. The method of splines with fixed knots is called regression splines [29, 39].

The B - spline basis consists of cubic splines specially parameterized. An extended set of knots is introduced to derive the formula for determining the j-th B – spline basis function of degree d:

$$\xi^* = (\xi_{-d}, \ldots, \xi_0, \xi, \xi_{K+1}, \ldots, \xi_{K+d+1}) \tag{8}$$

for $j = -d, \ldots, K + d$. Then recursion is applied:

$$B_{j,0}(x) = \begin{cases} 1 & if\ x \in \left[\xi_j, \xi_{j+1}\right) \\ 0 & if\ x \notin \left[\xi_j, \xi_{j+1}\right) \end{cases} \tag{9}$$

whereby:

$$B_{j,0}(x) \equiv 0 \tag{10}$$

if: $\xi_j = \xi_{j+1}$. Then - *j - th* function of degree *d* of the B – spline basis is calculated from the Mansfield - de Boor - Cox formula:

$$B_{j,d}(x) = \frac{x - \xi_j}{\xi_{j+d} - \xi_j} B_{j,d-1}(x) + \frac{\xi_{j+d+1} - x}{\xi_{j+d+1} - \xi_{j+1}} B_{j+1,d-1}(x) \tag{11}$$

where: $j = -d, \ldots, K + d - s$, while $s=1, \ldots, d$.

The piecewise B - basis polynomial splines $B_{j,d}$ with knots $\xi^*$ on the interval $(\xi_j, \xi_{j+d+1})$, satisfy, i.a., the following conditions:

$$a / B_{j,d+1}(x) > 0 \quad \forall x \in \left(\xi_j, \xi_{j+d+1}\right),$$
$$b / B_{j,d+1}(x) > 0, \forall j\ and\ \forall x,$$
$$c / \sum_{j}^{K+d+1} B_{j,d+1} = 1\ \forall x \in \left[\xi_0, \xi_{K+1}\right],$$

d/$B_{i,d+1}$ is a piecewise polynomial spline of degree d with knots in $\xi_1, \ldots, \xi_K$,

e/For internal knot number $k \ge 1$ functions $B_{j,d+1}$ belong to class $C^{m-2}(R)$, and $m < d + 1$.

The formula [11] will be used below to find an example of a basis function. In the practice of using regression splines, the plot of the model function is usually taken as the result of the calculation due to the complexity of the relationship under study.

***(2) Use of B - splines for description of the relationship between temperature of sample surface and heating time***

Both the variable "Time" and the variables "Temperature" and "Mass" are continuous variables. The values of these variables are in the intervals:

- "Time" xS ∈ [0,209967.09], s,
- "Temperature" T ∈ [295.8,1326.6], K,
- "Mass" M ∈ [150.60,264.94], g.

For the sample whose calcination results were used for the calculations in this paper, the relationships between the above variables are shown in Fig. 3. and Fig. 4. The variable "Time" in Fig. 3. and Fig. 4. is denoted by "τ". The two response variables in the function are denoted by the symbols yT and yM.

To replace the scatterplots shown in Fig. 3. and Fig. 4. by polynomial splines from the B - spline basis, the functions bs() and ns()are used from the package *splines* of the R environment for statistical computing. To achieve the target under consideration, the value of df in both functions is given. The value of df corresponds to the number of degrees of freedom. The number of internal knots $\xi$ for the function bs() is determined using equation:

$$\xi = df - d - \mathbb{1}_{intercept=TRUE} \tag{12}$$

where: df corresponds to the number of degrees of freedom, d is the degree of the partial polynomial, $\mathbb{1}$ is the component resulting from the presence of a constant term (intercept = TRUE) in the equation of the spline. Whereas the number of internal knots for the ns() function is calculated from the formula:

$$\xi = df - 1 - \mathbb{1}_{intercept=TRUE} \quad (13)$$

The imposition of the polynomial spline bs(splines) with parameter, e.g. df = 7 on the scatterplot, shown in Fig. 3., is done with the command:

```
> lines(xS,fitted(lm(yT~bs(xS,df=7,intercept=
TRUE))),lwd=2,col="black")
```

The result of applying this command is seen in the left part of Fig. 5. The linear model in which the dependent variable is the sample surface temperature and the explanatory variable is the result of calling the function bs(xS) with selected different numbers of degrees of freedom df:

```
> bT7<- lm(yT~bs(xS,df=7,intercept=TRUE))
```

does not reflect the shape of the scatterplot. Increasing the value of df leads to an increase in the number of intervals $\xi_j$, $\xi_{j+d+1}$ in the domain of the polynomial spline, which, with a chosen degree of polynomial, leads to a better fit of the spline to the scatterplot. Increasing the value of df from 7 to 15 results in a better fit of the spline and the scatterplot of the sample surface temperature measurements during heating as seen in the right-hand part of Fig. 5.

The selection of the number of degrees of freedom df for the best fit of the polynomial spline plot to the scatterplot of the measurement points with the smallest possible value of df is made on the basis of the Akaike information criterion (AIC) [29, 41]. For this purpose, the AICcmodavg package is used in the R computing environment. In the range of values df∈ [7, 15], the set of linear models shown below is built:

```
> bT7<- lm(yT~bs(xS,df=7,intercept=TRUE))
…
> bT15<- lm(yT~bs(xS,df=15,intercept=TRUE))
```

They are then ranked as shown in Table 3, which is obtained with the following commands below:

```
> <- list(bT7, …, bT15)
> model.namesbT <- c('bT7', …, 'bT15')
> aictab(cand.set = modelsbT, modnames =
model.namesbT) #Tablica 1
```

K is the assumed number of parameters of the linear regression model shown in Table 3. It was decided that, for example, the model bT15 would consist of 16 terms. To calculate the value of K, the assumed number of terms in the model should be increased by 1, due to the independent choice of degree of the polynomial function, e.g., degree = 3, as in the present case. Therefore, in the model bT15, the value of K=15+1=16, as can be seen in Table 3. The number of 15 terms in the model is shown in detail later in the paper. The values of the information criterion [29, 41] are found in column AICc and are used to classify the models. The lower the value of the criterion, the better the model fits the data. The AICc criterion is an adjusted AIC criterion due to the small sample size. However, it is considered [42] that it should also be applied to samples of any size. The AICcWt weight is the proportion of the predictive power of a given model in relation to the total predictive power of the full set of models. Cum.Wt is the sum of the weights of criterion AICc. In the analysed case, the best model contains 100 % of the predictive power of the set of tested models. LL is a measure of the goodness of fit of the model to the measurement results calculated using the maximum likelihood method. The AICc criterion is calculated using K and LL. From the LL values in Table 3, it can be seen that the bT15 model is characterised by the maximum value of the maximum likelihood estimator LL.

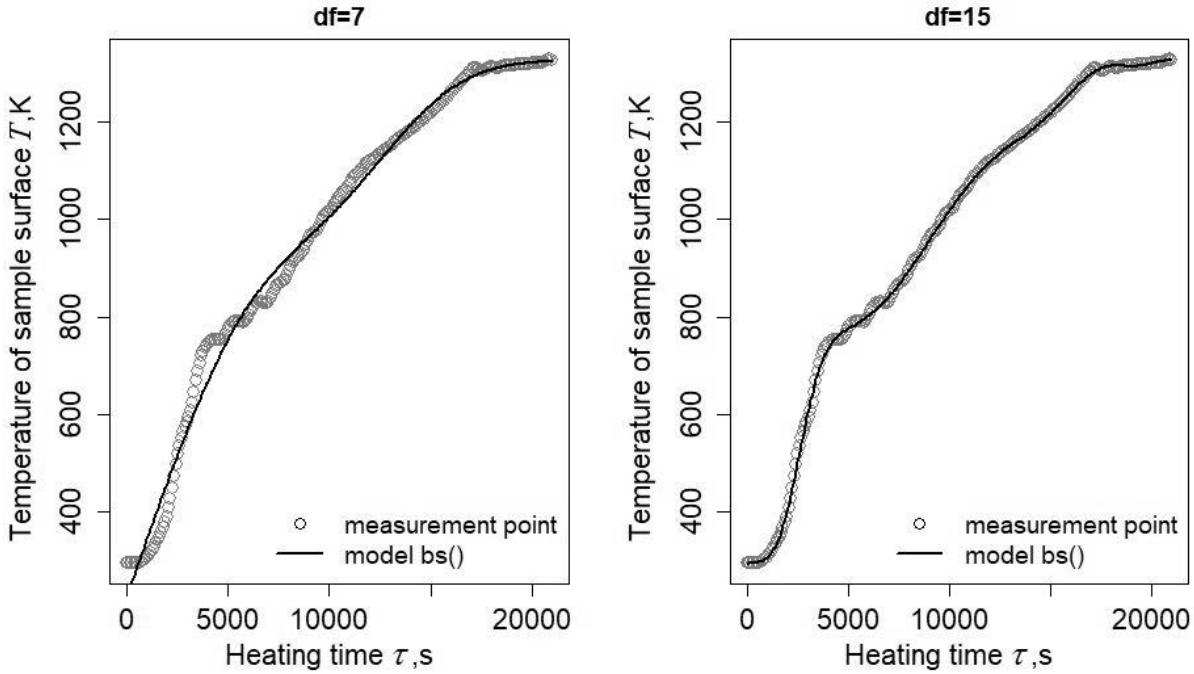


**Fig. 5:** Comparison of the fitted values of sample surface temperature for the models containing terms bs with various degrees of freedom df.

**Table 3:** Ranking of bs() models describing the correlation between surface temperature vs. sample heating time made using the AICc criterion.

| Model | K | AICc | Delta_AICc | AICcWt | Cum.Wt | LL |
|---|---|---|---|---|---|---|
| > bT15 | 16 | 1484,53 | 0,00 | 1 | 1 | -725,02 |
| > bT14 | 15 | 1529,95 | 45,42 | 0 | 1 | -748,88 |
| > bT13 | 14 | 1676,84 | 192,31 | 0 | 1 | -823,47 |
| … | | | | | | |
| > bT7 | 8 | 2259,74 | 775,21 | 0 | 1 | -1121,55 |

In the same way, the ns() models of the correlation between surface temperature and heating time of the specimen according to the AICc criterion were ranked. The results of the calculations for both bs() and ns() models are graphically presented in the dot plot shown in Fig. 6. Based on the results shown in Fig. 6, models bs(…, df=15, 6 …) and ns(…, df=13,…) were selected to describe the dependence of the sample surface temperature vs. heating time. Both selected models are characterised by the lowest value of the AICc criterion of the analyzed correlation, although taking into account the small difference of the AICc values of the models bs(…,df=14, …) and bs(…, df=15, …), the model with the parameter df = 14 can be selected. Similarly, the model with df = 12 can be selected in the case of the ns() models.

By assuming the model bs(…, df=15, …) as the best fit, a test of statistical significance of the estimators $\hat{\beta}$ of the model and the new model variables is performed. For this purpose, a new explanatory variable $x_i \in [0,1]$ with $i \in [1,235]$ is introduced, referring to the 235 measurements taken during the experiment. At the same time, using the percentiles listed in the notes to the regression matrix of the bT15u model, the internal knots for the bT15s model with the new explanatory variable x are determined. The values of the bT15s model coefficients are obtained with the following commands:

```
> bT15u<-bs(xS,df=15,intercept=TRUE)
> bT15u
> x<-seq(from=0, to=1, length=235)
> knotsbT15u<-c(0.08333333,0.1666667,0.25,
0.3333333,0.4166667,0.50,0.5833333,
0.6666667,0.75,0.8333333,0.9166667)
> bT15s<-bs(x, degree=3, knots=knotsbT15u,
intercept=T)
>fitT<-lm(yT~bs(x,degree=3,knots=knotsbT15u))
> fitT
> summary(fitT)
```

Table 4 contains the $\hat{\beta}$ estimators for the 14 terms of the model bs(…,df=15,…) written using the cubic B – spline basis functions. The results of their statistical significance tests are also shown. The study area of the independent variable was divided into 12 intervals using 11 internal knots. Table 4 shows the p-value, which indicates the statistical significance of the new model variables.

A similar test was carried out for model ns(…, df=13,…), the result of which is analogous. The models bs(…, df=15, …) and ns(…, df=13,…) are shown in Fig. 7 with the plots. The convergence of the two models is shown in Fig. 7., which, in conjunction with the right-hand part of Fig. 5., indicates a good fit of the two models and the measurement results.

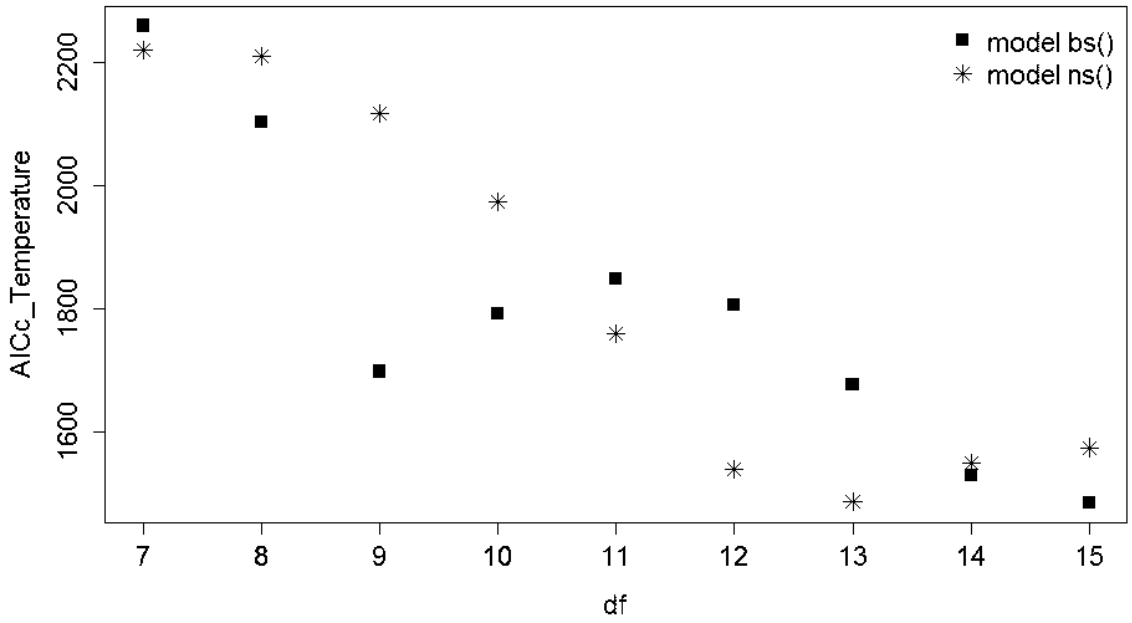


**Fig. 6:** AICc criterion values for the models of sample surface temperature during heating with application of bs and ns functions and various number of degrees of freedom df.

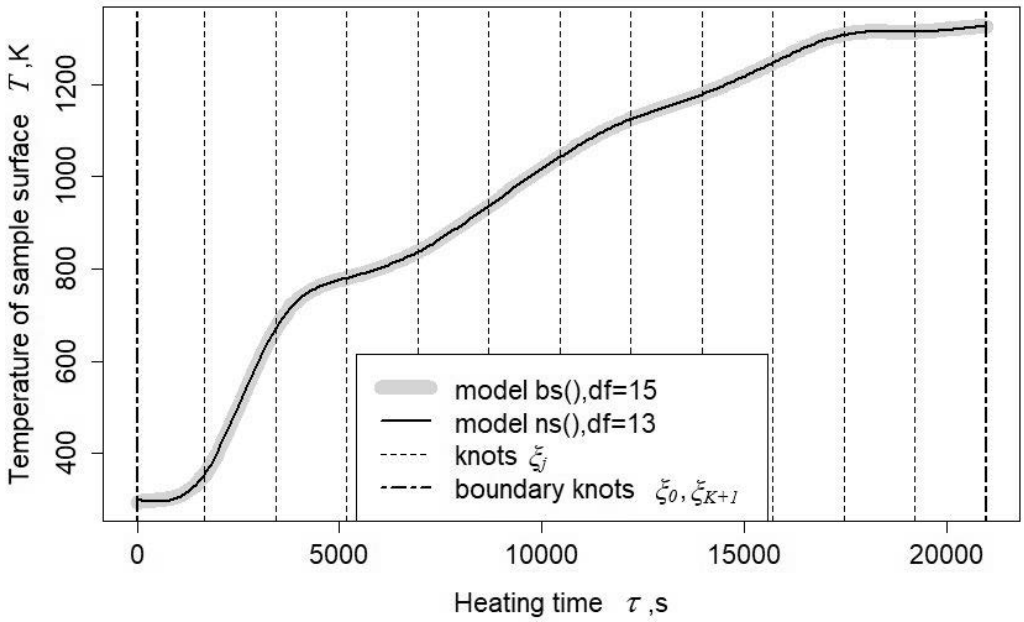


**Fig. 7:** Comparison of the fitted values of sample surface temperature for the chosen models containing the terms of bs(…,df=15,…) and ns(…,df=13,…) functions.

**Table 4:** Statistical significance test results for: $\hat{\beta}$ estimators of the bs() model terms of sample surface temperature vs. sample heating time relationship and of the new variables.

Call:
1m(formula = yT - bs(x, degree = 3, knots = knotsbT15u))

Residuals:

| Min | 1Q | Median | 3Q | Max |
|---|---|---|---|---|
| -20,2650 | -2,2009 | 0,0975 | 2,1715 | 14,3334 |

Coefficients:

| | Estimate Std | Error | t value | Pr(>\|t\|) |
|---|---|---|---|---|
| (Intercept) | 293,481 | 3,524 | 83,275 | < 2e-16 *** |
| bs(x, degree = 3, knots = knotsbT15u)1 | 9,557 | 6,643 | 1,439 | 0,152 |
| bs(x, degree = 3, knots = knotsbT15u)2 | -27,601 | 4,427 | -6,235 | 2,28e-09 *** |
| bs(x, degree = 3, knots = knotsbT15u)3 | 454,450 | 5,056 | 89,888 | < 2e-16 *** |
| bs(x, degree = 3, knots = knotsbT15u)4 | 482,595 | 4,322 | 111,657 | < 2e-16 *** |
| bs(x, degree = 3, knots = knotsbT15u)5 | 535,257 | 4,602 | 116,298 | < 2e-16 *** |
| bs(x, degree = 3, knots = knotsbT15u)6 | 642,408 | 4,422 | 145,267 | < 2e-16 *** |
| bs(x, degree = 3, knots = knotsbT15u)7 | 754,101 | 4,511 | 167,164 | < 2e-16 *** |
| bs(x, degree = 3, knots = knotsbT15u)8 | 839,341 | 4,465 | 187,990 | < 2e-16 *** |
| bs(x, degree = 3, knots = knotsbT15u)9 | 880,634 | 4,502 | 195,592 | < 2e-16 *** |
| bs(x, degree = 3, knots = knotsbT15u)10 | 953,073 | 4,529 | 210,448 | < 2e-16 *** |
| bs(x, degree = 3, knots = knotsbT15u)11 | 1031,325 | 4,683 | 220,221 | < 2e-16 *** |
| bs(x, degree = 3, knots = knotsbT15u)12 | 1011,389 | 5,260 | 192,287 | < 2e-16 *** |
| bs(x, degree = 3, knots = knotsbT15u)13 | 1031,962 | 5,409 | 190,779 | < 2e-16 *** |
| bs(x, degree = 3, knots = knotsbT15u)14 | 1031,610 | 4,984 | 207,002 | < 2e-16 *** |

Signif. codes: 0 '***' 0,001 '**' 0,01 '*' 0,05 '.' 0,1 ' ' 1

Residual standard error: 5,471 on 220 degrees of freedom
Multiple R-squared: 0,9997, Adjusted R-squared: 0,9997
F-statistic: 5,608e+04 on 14 and 220 DF, p-value: < 2,2e-16

It follows from the properties of the ns() function that for the same number of degrees of freedom, a larger number of knots is generated in the case of the ns() function, which usually results in a better model fit to the measurement results. In other words, an increase in the number of degrees of freedom results in greater variability in the model fit to the scatterplot of the measurement results as noted by Hastie *et al.* [29] and Lis [39].

### *(3) Use of B – splines for description of the relationship between thermal dissociation rate and temperature of sample surface*

Focusing further on the bs() models, a model of thermal dissociation rate of a limestone sample vs. sample surface temperature was fitted in an analogous way. The model was fitted for the description of the results of the calculation performed on the basis of the measurement results:

```
> fitbT9ru<-lm(DissRate~bs(x,degree=3,knots=
knotsbT9r))
```

The fit of the linear bT9ru model to the measurement and calculation results is shown in Fig. 8, while Table 5 shows the calculation results of $\hat{\beta}$ estimators of the bT9ru model terms together with the result of their statistical significance test. The p-value is also shown and indicates the statistical significance of the new model variables.

### *(4) Use of B-splines for description of the relationship between sample mass and heating time*

#### (a) *Choice of a linear model for prediction of sample mass and analytical expression of the B – spline basis functions*

The analysis of the calculation results of the calcined sample mass vs. heating time relationship is given below. Similarly as before, it was found that the best description of the relationship under study is given by the models bs(…,df=10,…) and ns(…,df=9,…). Their comparison is shown in Fig. 9. The plots of the models do not show any significant differences. Therefore, further analysis will be conducted for the bs(…,df=10,…) model.

**Table 5:** Statistical significance test results for: $\hat{\beta}$ estimators of the bs() model terms of sample thermal dissociation rate vs. sample surface temperature during heating and of the new variables.

Call:
1m(formula = DissRate ~ bs(x, degree = 3, knots = knotsbT9r))

Residuals:

| Min | 1Q | Median | 3Q | Max |
|---|---|---|---|---|
| -0,0125660 | -0,0004851 | 0,0000269 | 0,0006129 | 0,0090426 |

Coefficients:

| | Estimate | Std. Error | t value | Pr(>\|t \|) |
|---|---|---|---|---|
| (Intercept) | -2,489e-04 | 1,043e-03 | -0,239 | 0,81170 |
| bs(x, degree = 3, knots - knotsbT9r)1 | 6,770e-04 | 1,939e-03 | 0,349 | 0,72735 |
| bs(x, degree = 3, knots - knotsbT9r)2 | -8,534e-05 | l,256e-03 | -0,068 | 0,94587 |
| bs(x, degree = 3, knots = knotsbT9r)3 | 8,642e-04 | 1,474e-03 | 0,586 | 0,55817 |
| bs(x, degree - 3, knots - knotsbT9r)4 | -8,782e-04 | 1,261e-03 | -0,697 | 0,48670 |
| bs(x, degree - 3, knots = knotsbT9r)5 | 1,803e-02 | 1,396e-03 | 12,918 | < 2e-16 *** |
| bs(x, degree = 3, knots = knotsbT9r)6 | 2,275e-02 | 1,488e-03 | 15,296 | < 2e-16 |
| bs(x, degree = 3, knots = knotsbT9r)7 | -6,848e-04 | 1,580e-03 | -0,434 | 0,66501 |
| bs(x, degree = 3, knots = knotsbT9r)8 | 4,871e-03 | 1,469e-03 | 3,316 | 0,00107 ** |

Signif. codes: 0 '***' 0,001 '**' 0,01 '*' 0,05 '.' 0,1 ' ' 1

Residual Standard error: 0,002153 on 226 degrees of freedom

Multiple R-squared: 0,914, Adjusted R-squared: 0,9109

F-statistic: 300,1 on 8 and 226 DF, p-value: < 2,2e-16

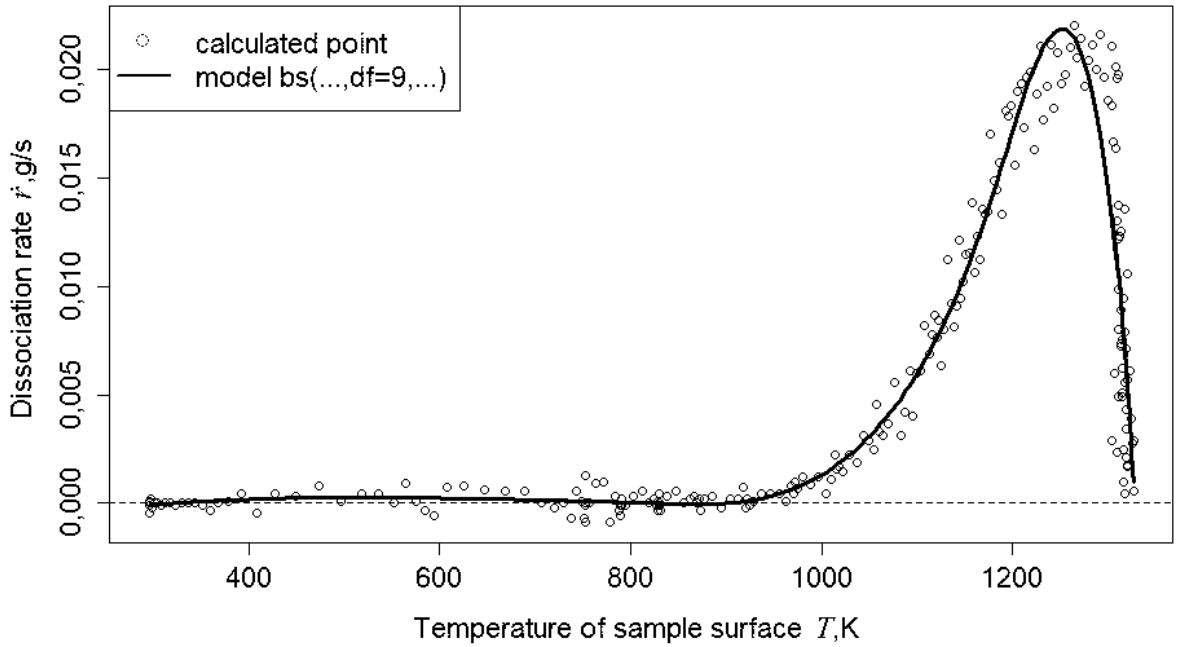


**Fig. 8:** Dissociation rate of sample mass depending on the surface temperature of the sample during sample heating.

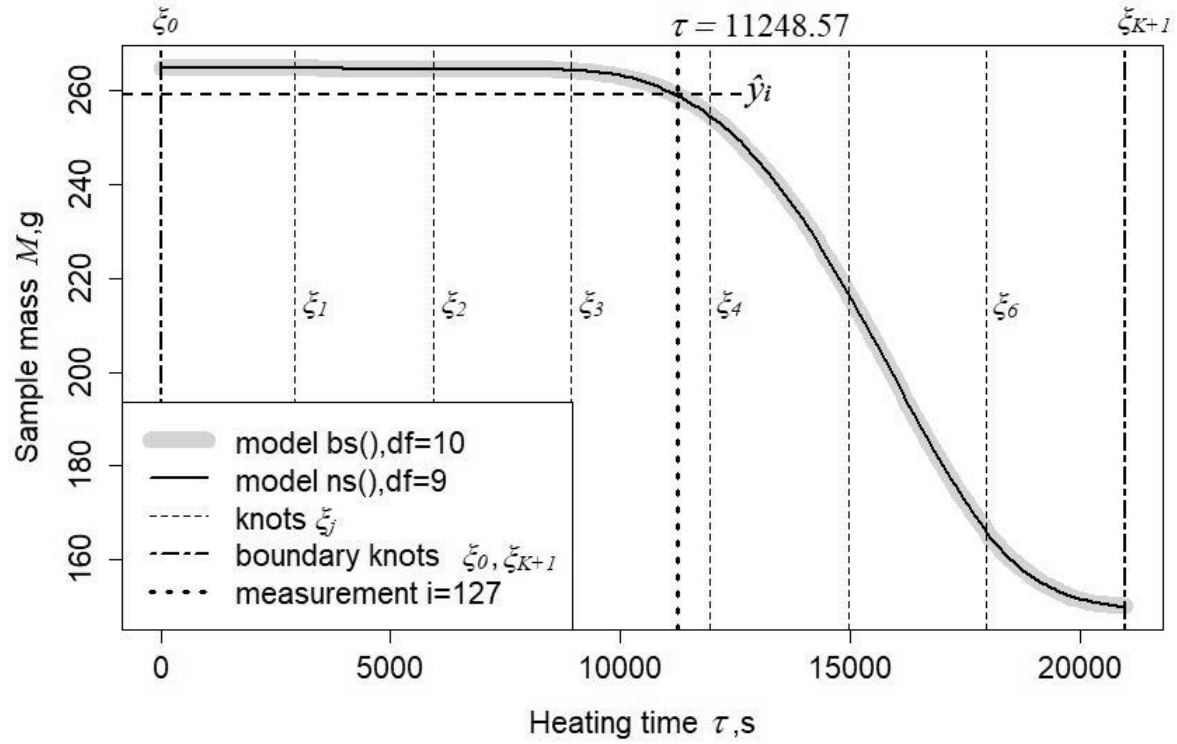


**Fig. 9:** Comparison of the fitted values of sample mass for the chosen models containing terms bs and ns with the given number of degrees of freedom df.

The statistical significance examination of the $\hat{\beta}$ estimators of the bs(…,df=10,…) model terms and the new variables is shown in Table 6. The nine model terms written using cubic basis B -splines are also shown in Table 6. The result of their statistical significance test is also shown. The domain of the independent variable was divided into 7 knot spans using 6 internal knots as shown in Fig. 9. Table 6 also shows the p-value, which indicates the statistical significance of the new model variables.

A regression matrix of dimension 235×10 is generated with the commands:

```
> model.splinesbM10<-bs(xS,df=10,intercept=TRUE)
>print(model.splinesbM10)
```

235 is the number of measurements performed. The number of columns is the model basis functions number. The example of these basis functions values for measurement, e.g. I = 127, is shown in Table 7. This example is called with the command:

```
>print(model.splinesbM10 127,)
```

**Table 6:** Statistical significance test results of the $\hat{\beta}$ estimators of bs(…,df=10,…) model of sample mass vs. sample heating time relationship and of the new variables.

Call:
1m(formula = yM ~ bs(x, df = 10, knots = knotsbM10))

Residuals:

| Min | 1Q | Median | 3Q | Max |
|---|---|---|---|---|
| -0,81369 | -0,09386 | -0,00649 | 0,09611 | 0,69502 |

Coefficients:

| | Estimate | Std. Error | t value | pr(> t) |
|---|---|---|---|---|
| (Intercept) | 264,87264 | 0,11705 | 2262,807 | < 2e-16 *** |
| bs(x, df = 10, knots = knotsbM10)1 | 0,17576 | 0,21800 | 0,806 | 0,420961 |
| bs(x, df = 10, knots = knotsbM10)2 | -0,06728 | 0,14174 | -0,475 | 0,635476 |
| bs(x, df = 10, knots = knotsbM10)3 | -0,55340 | 0,16529 | -3,348 | 0,000954 *** |
| bs(x, df = 10, knots = knotsbM10)4 | 0,24589 | 0,14090 | 1,745 | 0,082331. |
| bs(x, df = 10, knots = knotsbM10)5 | -4,19399 | 0,15212 | -27,570 | < 2e-16 *** |
| bs(x, df = 10, knots = knotsbM10)6 | -44,03747 | 0,15009 | -293,406 | < 2e-16 *** |
| bs(x, df = 10, knots = knotsbM10)7 | -107,68368 | 0,17220 | -625,332 | < 2e-16 |
| bs(x, df = 10, knots = knotsbM10)8 | -114,65053 | 0,17513 | -654,674 | < 2e-16 |
| bs(x, df = 10, knots = knotsbM10)9 | -114,73249 | 0,16591 | -691,522 | < 2e-16 |

Signif. codes: 0 '***' 0,001 '**' 0,01 '*' 0,05 '.' 0,1 ' ' 1

Residual Standard error: 0,226 on 225 degrees of freedom
Multiple R-squared: 1, Adjusted R-squared: 1
F-statistic: 8,805e-05 on 9 and 225 DF, p-value: < 2,2e-16

The measurement I = 127 performed at $\tau_{127} = 11248.57$ s of the sample calcination time is marked in Fig. 9. The selected value of the explanatory variable is in the knot span $[\xi_3,\xi_4)$ as is shown in Fig. 9. An example of the model response value calculation, i.e. the predicted sample weight $\hat{y}_{127}$, to the measured value $y_{127}$ for the explanatory variable $\tau_{127}$ using the values of the basis functions stored in Table 7 is shown below. For finding non-zero basis functions in the selected knot span that will be used to calculate the predicted sample mass, rule (40) is applied:

On any knot span $[\xi_j,\xi_{j+1})$ at most d+1 degree d basis functions are non-zero, namely:

$$B_{j-d,d}(x), B_{j-d+1,d}(x), B_{j-d+2,d}(x), \ldots, B_{j-1,d}(x), B_{j,d}(x) \tag{14}$$

which, in the considered knot span for $j = 3$ and $d = 3$, gives the following functions:

$$B_{0,3}(x), B_{1,3}(x), B_{2,3}(x), B_{3,3}(x) \tag{15}$$

(b) ***Analytic expression of the B – spline basis functions***

The analytic expression of the function [15] can be determined with the triangle method shown in Fig. 10. The symbol for the knot span, i.e. $[\xi_3,\xi_4)$ in which the non-zero basis functions are sought, is the vertex of the isosceles triangle $\alpha_1\Delta[\xi_3,\xi_4)\alpha_2$, whose sides are drawn with a dashed line and they are shown in Fig. 10. The sought non-zero basis functions of degree d = 3 are located at the base $\alpha_1\alpha_2$ of the triangle $\alpha_1\Delta[\xi_3,\xi_4)\alpha_2$, and they are indicated by arrows in Fig. 10. These functions are applied in a linear model of the sample mass predicted value $\hat{y}$ at a selected moment belonging to the knot span $[\xi_3, \xi_4)$.

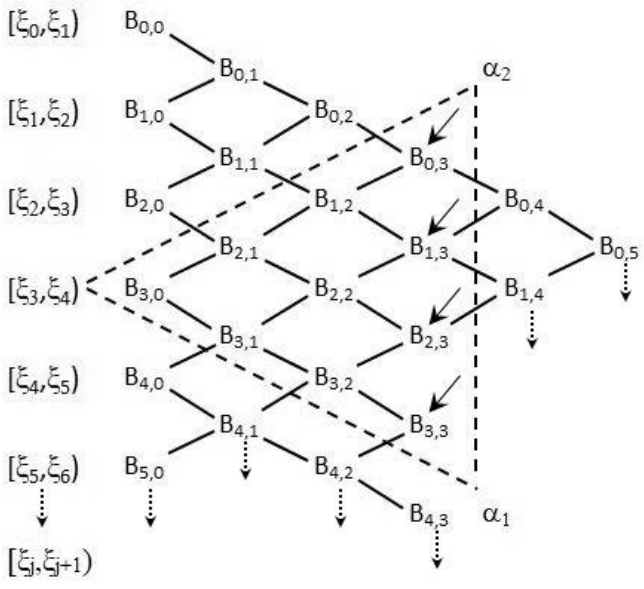


**Fig. 10:** Scheme for finding non-zero basis functions of degree d = 3 in the knot span $[\xi_3, \xi_4)$.

As an example, the formula of the cubic basis function $B_{0,3}$ derived using the recursive formula [11] is written below and its value is calculated for the measurement I = 127, which belongs to the knot span $[\xi_3, \xi_4)$. The form of the function is:

$$B_{0,3}(x) = \frac{(\xi_4 - x_i)^3}{(\xi_4 - \xi_1)(\xi_4 - \xi_2)(\xi_4 - \xi_3)} \tag{16}$$

The result of the calculation performed in R for measurement I = 127 after using the command:

> x [127]

is the value: $x_{127}$ = x[127] = 0.5384615.

Furthermore, the regression matrix containing the values of the basis functions generated by the R calculation environment for the model bs(x, df = 10, intercept = T) contains the following values of the knots used in the formula [16]:

$\xi_1 = 0.1428571$, $\xi_2 = 0.2857143$, $\xi_3 = 0.4285714$,

$\xi_4 = 0.5714286$, $\xi_5 = 0.7142857$, $\xi_6 = 0.8571429$. .

After the insertion of the above values into the formula [16] of the cubic basis function, its value $B_{0,3}$ = 0.002048252 = bs3 is obtained. For rounding accuracy, it is the value of this function for measurement I = 127 shown in Table 7. The above basis function in the model shown in Table 6 is written as the function bs(x, df = 10, knots = knotsbM10)3, and its shorter version written is bs3. Thus, the values of the other basis functions indicated in Fig. 10. and shown in Table 7 are as follows:

$B_{1,3}$ = 0.302533758 = bs4, $B_{2,3}$ = 0.619556972 = bs5, $B_{3,3}$ = 0.075861023 = bs6.

It is worth noting that the sum of the computed values of the basis functions is 1. The plots of these functions in domain $x_i \in [0, 1]$ are shown in Fig. 11.

Knowing the values of the basis functions for the variable $x_{127}$ located in the knot span $[\xi_3,\xi_4)$ at time $\tau$=11248.57 s of the measurement, the predicted value of the sample mass is calculated using the bM10 model. The general form of this model given in Table 6 is as follows:

$$\begin{aligned}\hat{y}_i = {} & 264.87264 + 0.17576 \times \text{bs1} - 0.06728 \times \text{bs2} - \\ & 0.55340 \times \text{bs3} + 0.24589 \times \text{bs4} - 4.19399 \times \text{bs5} - \\ & 44.03747 \times \text{bs6} - 107.68368 \times \text{bs7} - \\ & 114.65053 \times \text{bs8} - 114.73249 \times \text{bs9}\end{aligned} \tag{17}$$

which in the considered calculation case for the knot span $[\xi_3,\xi_4)$ is simplified to the form:

$$\begin{aligned}\hat{y}_i = {} & 264.87264 - 0.55340 \times \text{bs3} + 0.24589 \times \text{bs4} - \\ & 4.19399 \times \text{bs5} - 44.03747 \times \text{bs6}\end{aligned} \tag{18}$$

as only these basis functions are non-zero in the knot span $[\xi_3,\xi_4)$, as shown in Fig. 11.

**Table 7:** Row *i* = 127 of the degree 3 basis functions matrix of the bM10r model.

| 1 | 2 | 3 | 4 | 5 |
|---|---|---|---|---|
| 0,000000000 | 0,000000000 | 0,000000000 | 0,002047923 | 0,302527103 |
| 6 | 7 | 8 | 3 | 10 |
| 0,619560448 | 0,075864526 | 0,000000000 | 0,000000000 | 0,000000000 |

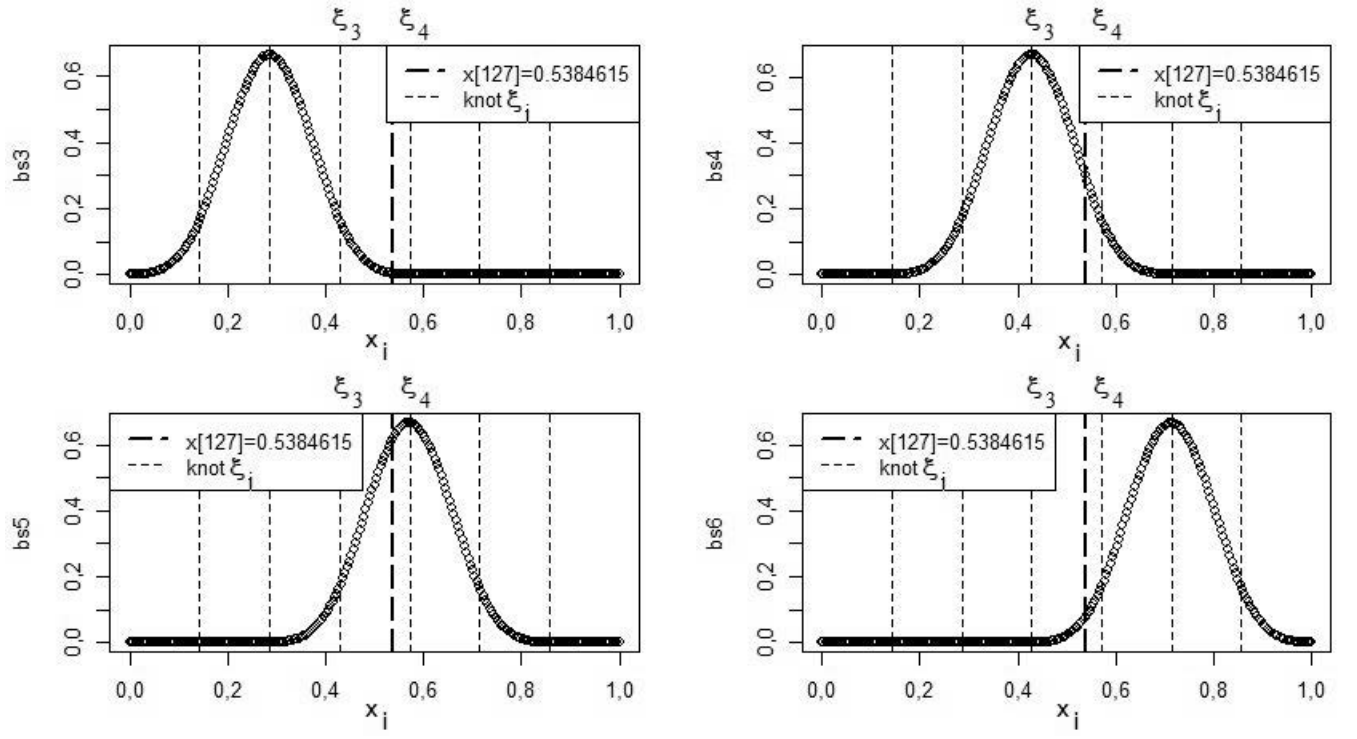


**Fig. 11:** Non-zero cubic basis functions bs3, bs4, bs5, bs6 in knot span $[\xi_3,\xi_4)$.

By inserting the values bs3, bs4, bs5, bs6 contained in the model basis function matrix into Equation [18], the predicted value of the sample mass at the moment corresponding to measurement I = 127 is calculated to be $\hat{y}_{127} = 258.86$ g. The measured sample mass was $y_{127} = 259.56$ g. Hence the residual is $y_{127} - \hat{y}_{127} = 0.70$ g.

The other basis functions have the form shown in Equations [17 – 19]:

$$B_{1,3}(x_i) = -\left[\begin{array}{l} \dfrac{(\xi_1 - x_i)(\xi_4 - x_i)^2}{(\xi_4 - \xi_1)(\xi_4 - \xi_2)(\xi_4 - \xi_3)} + \\ \dfrac{(\xi_2 - x_i)(\xi_4 - x_i)(\xi_5 - x_i)}{(\xi_4 - \xi_2)(\xi_4 - \xi_3)(\xi_5 - \xi_2)} + \\ \dfrac{(\xi_3 - x_i)(\xi_5 - x_i)^2}{(\xi_4 - \xi_3)(\xi_5 - \xi_2)(\xi_5 - \xi_3)} \end{array}\right] \tag{19}$$

$$B_{2,3}(x_i) = -\left[\begin{array}{l} \dfrac{(x_i - \xi_4)(x_i - \xi_2)^2}{(\xi_4 - \xi_2)(\xi_4 - \xi_3)(\xi_5 - \xi_2)} + \\ \dfrac{(x_i - \xi_2)(x_i - \xi_3)(x_i - \xi_5)}{(\xi_4 - \xi_3)(\xi_5 - \xi_2)(\xi_5 - \xi_3)} + \\ \dfrac{(x_i - \xi_6)(x_i - \xi_3)^2}{(\xi_4 - \xi_3)(\xi_5 - \xi_3)(\xi_6 - \xi_3)} \end{array}\right] \tag{20}$$

$$B_{3,3}(x) = \frac{(x_i - \xi_3)^3}{(\xi_6 - \xi_3)(\xi_5 - \xi_3)(\xi_4 - \xi_3)} \tag{21}$$

The sample heating time is a continuous variable. Therefore, the analytical form of the predicted calcined sample mass ŷ can be derived from the equations [16, 19 – 21]. Then the sample (grain, limestone lump) dissociation rate as a function of heating time for a given furnace chamber heating curve is the derivative of dŷ/dx.

The properties of lime depend, among other things, on the calcination time and the calcination temperature. Boyton [11] discusses, e.g. a significant effect of calcination time and temperature of limestone on the size of the specific surface area of the produced lime. He cites the results of a study in the value of the specific surface area changes of lime produced from limestone containing 98.5 % $CaCO_3$ calcined, e.g., at a temperature of about 1 093 °C over a period of 16 hours. The specific surface area of the lime decreased from a value of 1.8 to a value of 0.4 $m^2 \cdot g^{-1}$ during calcination. In turn, Oates [12] cites the results of a study of lime density as a function of temperature and calcination time. He shows an increase in lime density depending on the calcination time for each temperature used in the tests. For example, the density of lime produced from limestone with a high $CaCO_3$ content after about 3 hours of calcination at 1 100 °C equalled about 1.76 $g \cdot cm^{-3}$, and after 27 hours of calcination at the same temperature the density of the produced lime increased to the value of 2.03 $g \cdot cm^{-3}$.

*(c) Use of B – splines for description of the relationship between thermal dissociation rate vs heating time and surface temperature of calcinated sample*

A scatterplot of the sample thermal dissociation rate vs. heating time and surface temperature measurement results, using the measurement results shown in Fig. 3. and Fig. 4., is shown in Fig. 12. Therefore, in studies of calcination of limestone samples, it is useful to use the R program, which allows the construction of plots of the studied property limestone sample vs., e.g., two or more variables. As already mentioned, these measurements were conducted using the furnace heating curve shown in Fig. 2. The heated mixture of air and carbon dioxide with $c_{CO_2} = 45.16$ %vol. was flowed into the furnace heating chamber.

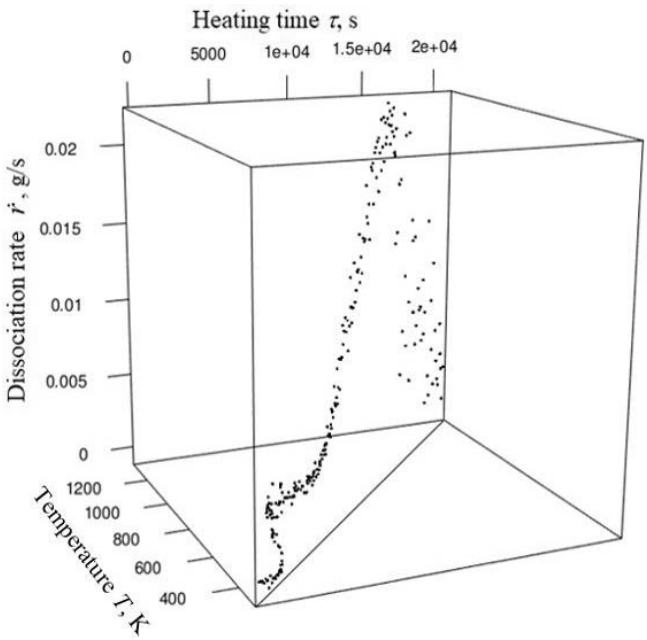


**Fig. 12:** Scatterplot of the calculated thermal dissociation rate of the limestone sample (Dissociation rate $\dot{r}$ $g \cdot s^{-1}$) as a function of the sample thermal dissociation time (Time $\tau$, s) vs. the sample surface temperature (Temperature $T$, K): heating curve according to Fig. 2, gas mixture with concentration $C_{CO_2} = 45.16$ %vol.

The diagram shown in Fig. 12 is constructed after loading the *Diss* package containing the results of own calculations and the *rgl* package from the set of packages contained in the R program by calling the function:

```
> plot3d(x=Diss$Temperature,y=Diss$Time,
z=Diss$Rate,
xlab="",ylab="",zlab="",cex.axis=2)
```

The shape of thefurnace heating curve depends on the selection of the heating rate of the furnace heating chamber within the assumed heating intervals. The heat transfer conditions in the heating chamber and the rate of thermal dissociation of the limestone sample also depend on the $CO_2$ concentration in the gas mixture entering the heating chamber. Therefore, based on determination of the ranges of these quantities, a scatterplot of the dissociation rate measured results of the calcined limestone sample can be drawn for the function $\dot{r} = f\left(T, \tau, c_{CO_2}\right)$.

## V. Conclusions

1. The temperature of the calcined surface of a large limestone sample (grains, limestone lump) and the degree of its conversion to lime are among the most important functions used in modelling of the thermal dissociation of charge for the production of lime.

2. A description of measurement results for the surface temperature and calcined mass of a large sample of limestone (grains, limestone lump) as a function of calcination time can be obtained using the cubic base B - splines contained in splines package of the R computational environment for statistical calculations and modelling.
3. A linear model of the temperature of the surface of a calcined sample prepared for given conditions of temperature, calcination time, and $CO_2$ concentration in the sample environment can be used to model the thermal dissociation of a limestone charge in the shaft of a selected lime kiln. Similarly a linear model of the predicted sample mass and analytical forms of functions from the B - spline basis in combination with their values contained in the regression matrix generated by the R program for a selected knot span of the function domain may be used for modelling of sample thermal decomposition.
4. The regression splines may be used for an analytical description of results obtained in thermal analysis methods, which are used to study changes of the properties of a substance occurring during its heating or cooling under different measurement conditions.

## NOMENCLATURE

| | |
|---|---|
| $B$ | = B-spline basis function |
| $K$ | = number of knots |
| $M$ | = degree of transformation of predictor |
| $N$ | = number of measurements |
| $T$ | = temperature |
| $X$ | = predictor |
| $Y$ | = response variable |
| $d$ | = degree of B – spline basis function |
| $df$ | = degree of freedom |
| $\dot{r}$ | = rate of thermal dissociation |
| $x$ | = measurement result of predictor |
| $y$ | = measurement result of response variable |
| $z$ | = charge layer thickness coordinate |
| $\hat{y}$ | = estimated value of response variable |
| $\alpha$ | = coefficient |
| $\beta$ | = parameter of predictor |
| $\hat{\beta}$ | = estimator of parameter |
| $\varepsilon$ | = random error |
| $\xi$ | = knot |
| $\sigma^2$ | = variance of error term |
| $\tau$ | = time |
| $\vartheta$ | = coefficient |

| | SUBSCRIPTS |
|---|---|
| $h$ | = heating time |
| $i$ | =measurement number |
| $j$ | =knot number |
| $t$ | =predictor number |

## References


1 Zawadzki, J., Bretsznajder, S.: Über den Verlauf der Reaktionen zwischen CaO und $CO_2$ sowie zwischen CaO und $SO_2$, *Bull. Acad. Pol. Sci. A.*, 271 – 286, (1932).

2 Zawadzki, J., Bretsznajder, S.: Zur Kenntnis der heterogenen Reaktionen vom Typus $A_{fest} + B_{Gas} \leftrightarrows C_{fest}$ , I. Abweichungen von der Konstanz des Gleichgewichtsdruckes, Scheinbare Gleichgewichte und deren Deutung, *Z. Phys. Chem.*, **B.22**, 60 – 78, (1933).

3 Zawadzki, J., Bretsznajder, S.: Zur Kenntnis der heterogenen Reaktionen vom Typus $A_{fest} + B_{Gas} \leftrightarrows C_{fest}$ , II. Kinetik der Carbonatbildung und Zersetzung, *Z. Phys. Chem.*, B.22, 79 – 96, (1933).

4 Zawadzki, J., Bretsznajder, S.: A contribution to the kinetics of reactions in which solid phases take part, *Bull. Acad. Pol. Sci. A.*, 60 – 64, (1946).

5 Bretsznajder, S.: O przebiegu reakcji typu $A_{ciało\ stat} + B_{gaz} \leftrightarrows C_{ciało\ stat}$, w/in Błasiak E. (*et al*. eds.), Kataliza i katalizatory, PWT, Warszawa, 1952.

6 Hills, A.W.D.: The mechanism of the thermal decomposition of calcium carbonate, *Chem. Eng. Sc.*, **23**, 297 – 320, (1968).

7 Pigoniowa, J., Gumiński, K., Statyka chemiczna, w/in Bielański A. *et al.* eds., Chemia fizyczna, PWN, Warszawa, 1980.

8 Yagi, S., Kunii, D.: Studies on combustion of carbon particles in flames and fluidized beds, Fifth Symposium (International) on Combustion, Van Nostrand Reinhold, New York, 1954.

9 Verma, C.L.: Simulation of lime shaft kilns using mathematical modelling, *Zement – Kalk – Gips*, **43**, [12], 576 – 582, (1990).

10 Khinast, J., Krammer, G.F., Brunner, Ch., Staudinger, G.: Decomposition of limestone: the influence of $CO_2$ and particle size on the reaction rate, *Chem. Eng. Sc.*, **51**, 623 – 634, (1996).

11 Boynton, R.S.: Chemistry and technology of lime and limestone. John Wiley & Sons, Inc., New York, Chichester, Brisbane, Toronto, 1980.

12 Oates, J.A.H.: Lime and Limestone. Chemistry and Technology, Production and Uses, Wiley-VCH, Weinheim, New York, Chichester, Brisbane, Singapore, Toronto, 1998.

13 Locher, G.: Mathematische Modelle zum Prozess des Brennens von Zementklinker, T.1: Reaktionen und Grundoperationen, *ZKG Int.*, **55**, [1], 29 – 38, (2002).

14 Locher, G.: Mathematische Modelle zum Prozess des Brennens von Zementklinker, T.2: Vorwärmer, Calcinator und Bypass, *ZKG Int.*, **55**, 39 – 50, (2002).

15 Martins, M.A., Oliveira, L.S., Franca, A.S.: Modellierung und Simulation der Kalksteincalcination im Drehofen, Part I, *ZKG Int.*, **55**, [4], 76 – 87, (2002).

16 Martins, M.A., Oliveira, L.S., Franca A.S.: Modellierung und Simulation der Kalksteincalcination im Drehofen, Part II, *ZKG Int.*, **55**, [5], 74 – 83, (2002).

17 Gordon, Y.M., Blank, M.E., Madison, V.V., Abovian, P.R.: New technology and shaft furnace for high quality metallurgical lime production, AsiaSteel 2003, India, 1, 1.b1.1 – 1.b.1.6, 2003.

18 Gordon, Y.M., Shvidkiy, V., Yaroshenko, Y.: Optimization of the design and operating parameters of shaft furnaces, METEC Congress, 3rd ICSTI, Düsseldorf, 2003.

[19] Stanmore, B.R., Gilot, P.: Review – calcination and carbonation of limestone during thermal cycling for $CO_2$ sequestration, *Fuel Process. Technol.*, **86**, 1707 – 1743, (2005).

[20] Georgakis, Ch., Chang, C.W., Szekely, J.: A changing grain size model for gas – solid reactions, *Chem. Eng. Sci.*, **34**, [8], 1072 – 1075, (1979).

[21] Bes, A.: Dynamic process simulation of limestone calcination in normal shaft kilns, Thesis (PhD), Otto-von-Guericke-Universität Magdeburg, **59 – 62**, 79 – 80, (2006).

[22] Clark, J.B., Hastie, J.W, Kihlborg, L.H.E., Metselaar, R., Thackeray M.M.: Definitions of terms relating to phase transitions of the solid state, *Pure & Appl. Chem.*, **66**, [3], 592, (1994).

[23] Specht, E.: Wärme- und Stoffübertragung in der Thermoprozesstechnik. Grundlagen, Berechnungen, Prozesse, Vulkan Verlag GmbH, Essen, 198 – 205, 484 – 502, (2004).

[24] Hallak, B., Herz, F., Specht, E., Gröpler, R., Warnecke, G.: Simulation of limestone calcination in normal shaft kilns – mathematical model, *ZKG*, **9**, 66 – 71, (2005).

[25] Hallak, B., Herz, F., Specht, E., Gröpler, R., Warnecke, G.: Simulation of limestone calcination in normal shaft kilns – Part 2: Influence of process parameters, *ZKG*, **10**, 46 – 50, (2015).

[26] Hallak, B., Herz, F., Specht, E., Gröpler, R., Warnecke, G.: Simulation of limestone calcination in normal shaft kilns – Part 3: Influence of particle size distribution and type of limestone, *ZKG*, **3**, 64 – 68, (2016).

[27] Piringer, H.: Lime shaft kilns, INFUB-11$^{th}$ European Conference on Industrial Furnaces and Boilers, INFUB-11, Energy Procedia 120, 75 – 95, 2017.

[28] Brown, M.E.: Introduction to thermal analysis. Techniques and application, 2.Ed., Kluwer Academic Publishers, New York, Boston, Dordrecht, London, Moscow, 1 – 12, (2004).

[29] Hastie, T., Tibshirani, R., Friedman, J.: The Elements of Statistical Learning: Data Mining, Inference, and Prediction, 2$^{nd}$ edit., New York: Springer, 139 – 161, 186 – 189, 203 – 232, (2009).

[30] Trzęsiok, J., Trzęsiok, M.: Nieparametryczne metody regresji, w/in Walesiak M., Gatnar E. (Sci.Ed.), Statystyczna analiza danych z wykorzystaniem programu R, Wyd.Nauk. PWN, Warszawa, 2002.

[31] R Core Team, R: A language and environment for statistical computing. R Foundation for Statistical Computing, Vienna, Austria, 2020.

[32] Kozłowski, S.: Surowce skalne Polski, Wyd. Geologiczne, Warszawa, 1986.

[33] Lech, R.: Thermal decomposition of limestone: Part 1 – Influence of properties on calcination time, *Sil. Ind.*, **71**, [7 – 8], 103 – 109, (2006).

[34] Lech, R.: Termiczny rozkład wapieni: Transport masy i ciepła, Polska Akademia Nauk, Oddział w Krakowie, *Ceramika*, **105**, 29 – 53, (2008).

[35] Aczel, A.D., Sounderpandian, J.: Statystyka w zarządzaniu, Wyd. Nauk. PWN SA, Warszawa, 2008.

[36] Neter, J., Wasserman, W., Whitmore, G.A.: Applied Statistics, 3 ed., Allyn & Bacon, Inc., Newton, 1988.

[37] Faraway, J.J.: Extending the linear model with R: Generalized Linear, Mixed Effects and Nonparametric Regression Models, 2 ed., CRC Press, Taylor & Francis Group: A Chapman & Hall Book, 2016.

[38] Hastie, T., Tibshirani, R.: Generalized additive models, *Stat Sci.*, **1**, [3], (1986).

[39] Lis, A.: Uogólnione modele addytywne z parametrem położenia, skali i kształtu, Praca magisterska, UW WMIM, 2011.

[40] Carl de Boor, C.: A practical guide to splines, New York: Springer-Verlag, 87 – 108, 2001.

[41] Davies, T.M.: The book of R. A first course in programming and statistics, No Starch Press, San Francisco, 2016.

[42] Hurvich, C.M., Tsai, C.-L.: Regression and Time Series Model Selection in Small Samples, *Biometrika*, **76**, 297 – 307, (1989.